Biochimica et Biophysica Acta 1847 (2015) 429–440

Contents lists available at ScienceDirect

Biochimica et Biophysica Acta

journal homepage: www.elsevier.com/locate/bbabio

# Species-dependent alteration of electron transfer in the early stages of charge stabilization in Photosystem I

Michael D. McConnell [a,b,c], Junlei Sun [d], Reza Siavashi [f], Andrew Webber [a,c], Kevin E. Redding [b,c,*], John H. Golbeck [d,e,**], Art van der Est [f,***]

[a] School of Life Sciences, Arizona State University, Tempe, AZ 85287, USA
[b] Department of Chemistry & Biochemistry, Arizona State University, Tempe, AZ 85287, USA
[c] Center for Bioenergy & Photosynthesis, Arizona State University, Tempe, AZ 85287, USA
[d] Department of Biochemistry and Molecular Biology, The Pennsylvania State University, University Park, PA 16802, USA
[e] Department of Chemistry, The Pennsylvania State University, University Park, PA 16802, USA
[f] Department of Chemistry, Brock University, St. Catharines, ON L2S 3A1, Canada

ARTICLE INFO

*Article history:*
Received 18 November 2014
Received in revised form 21 January 2015
Accepted 26 January 2015
Available online 3 February 2015

*Keywords:*
Photosynthesis
Photosystem I
Phylloquinone
Electron transfer
$A_0$

ABSTRACT

Electron transfer (ET) in Photosystem I (PS I) is bidirectional, occurring in two pseudosymmetric branches of cofactors. The relative use of two branches in the green alga *Chlamydomonas reinhardtii* and the cyanobacterium *Synechocystis* sp. PCC 6803 has been studied by changing the Met axial ligands of the chlorophyll *a* acceptor molecules, $A_{0A}$ and $A_{0B}$, to His. The nature of the effect on the ET is found to be species dependent. In *C. reinhardtii*, transient absorption and transient EPR data show that in the $M688H_{PsaA}$ variant, forward ET from $A_{0A}$ to the quinone, $A_{1A}$, is blocked in 100% of the PS I complexes. In contrast, in *Synechocystis* sp. PCC 6803, forward ET from $A_{0A}$ to $A_{1A}$ is blocked in only 50% of the PS I complexes, but in those PS I complexes in which electrons reach $A_{1A}$, further transfer to the iron–sulfur cluster $F_X$ is blocked. Similar species differences are found for the corresponding B-branch variants. One possible explanation of this behavior is that it is the result of two conformers in which an H-bond between the His side chain and the O1 carbonyl group of $A_1$ is either present or absent. The spectroscopic data suggest that the two conformers are present in nearly equal amounts in the *Synechocystis* sp. PCC 6803 variants, while only the conformer without the H-bond is present in the same variants of *C. reinhardtii*.



## 1. Introduction

In oxygenic photosynthesis, Photosystem I (PS I) uses light to transport electrons across a steep thermodynamic gradient from plastocyanin or cytochrome $c_6$ in the lumen to ferredoxin or flavodoxin in the stroma. Electron transfer from $P_{700}$ (a chlorophyll *a*/chlorophyll *a′* special pair) to $F_X$ (a [4Fe–4S] cluster) occurs along two branches of cofactors located at the interface of the PsaA and PsaB subunits [1,2] (Fig. 1). Each branch contains a pair of chlorophyll *a* molecules ($ec2_A/ec3_A$ or $ec2_B/ec3_B$) and a phylloquinone ($PhQ_A$ or $PhQ_B$). Spectroscopically, the $ec3_A$ and $ec3_B$ chlorophylls are referred to as $A_{0A}$ and $A_{0B}$ and the $PhQ_A$ and $PhQ_B$ phylloquinones are referred to as $A_{1A}$ and $A_{1B}$. Because both branches converge at $F_X$, their relative use is not apparent from inspection of the structure, but has been determined experimentally by making point mutations to amino acids in PsaA and PsaB that interact with specific cofactors in the A- and B-branches [3]. These studies have provided strong evidence that both branches are active, with reported lifetimes of ~200 ns and ~20 ns for electron transfer from $A_{1A}$ to $F_X$ and from $A_{1B}$ to $F_X$ in the A- and B-branches respectively. The relative activity of B-branch is species dependent and is estimated to be <20% in the cyanobacterium *Synechocystis* sp. PCC 6803 [4] but ~40% in the green alga *Chlamydomonas reinhardtii* [5,6].

Similar or identical mutations of the Met residues $M688_{PsaA}$ and $M668_{PsaB}$, which act as the axial ligands to chlorophylls $A_{0A}$ and $A_{0B}$, respectively, have been reported to produce different phenotypes in *Synechocystis* sp. PCC 6803 and *C. reinhardtii*. In the first study of the *C. reinhardtii* $M688H_{PsaA}$ and $M668H_{PsaB}$ variants, Fairclough et al. [7] observed that the EPR and ENDOR signals of photoaccumulated phyllosemiquinone were different in the two variants and that signals from the wild type were a mixture of those from the two variants. The authors of concluded that the mutations prevented electron transfer

*Abbreviations:* PS I, Photosystem I; DPIP, 2,6-dichlorophenolindophenol; Chl, chlorophyll; EPR, electron paramagnetic resonance; OOP-ESEEM, out-of-phase electron spin echo envelope modulation

* Correspondence to: K. Redding, Department of Chemistry & Biochemistry, Arizona State University, Tempe, AZ 85287, USA. Tel.: +1 480 965 0136.
** Correspondence to: J.H. Golbeck, Department of Biochemistry and Molecular Biology, The Pennsylvania State University, University Park, PA 16802, USA. Tel.: +1 814 865 1163.
*** Correspondence to: A. van der Est, Department of Chemistry, Brock University, St. Catharines, ON L2S 3A1, Canada. Tel.: +1 905 688 5550.
*E-mail addresses:* Kevin.Redding@asu.edu (K.E. Redding), jhg5@psu.edu (J.H. Golbeck), avde@brocku.ca (A. van der Est).

http://dx.doi.org/10.1016/j.bbabio.2015.01.011
0005-2728/

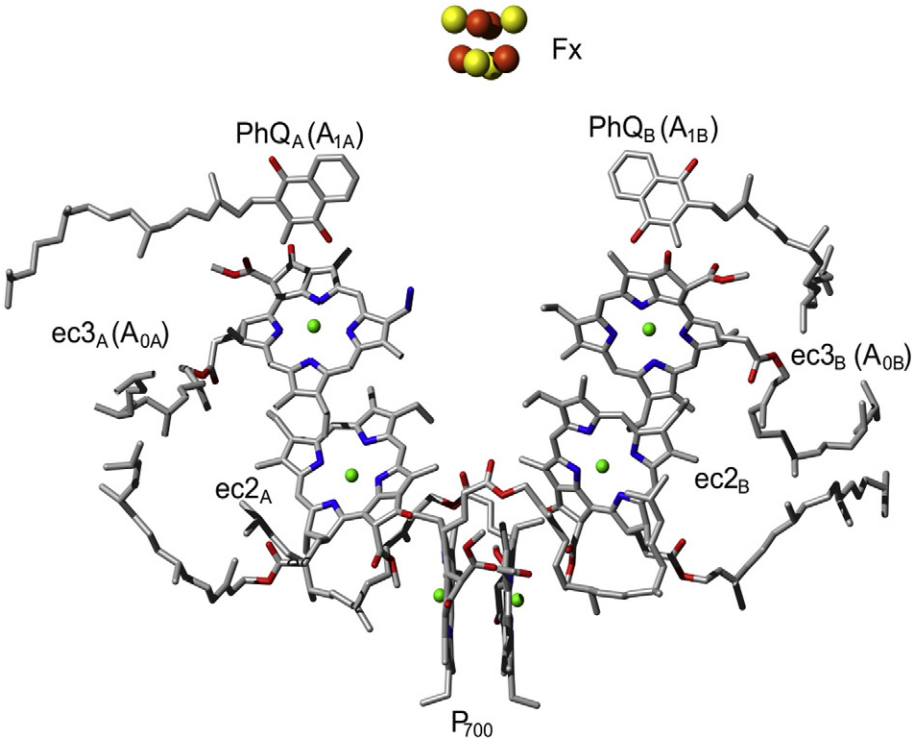


**Fig. 1.** Arrangement of the electron transfer cofactors in Photosystem I. The labels, $ec3_A$, $ec3_B$, $PhQ_A$ and $PhQ_B$ are the crystallographic nomenclature for the acceptors in the A- and B-branches. The labels $A_{0A}$, $A_{0B}$, $A_{1A}$ and $A_{1B}$ are the corresponding spectroscopic labels. The figure was constructed from the 2.5-Å resolution X-ray structure of PS I from *T. elongatus* (PDB ID: 1JB0) [2] using molmol [39].

past $A_0$ in the branch carrying the mutation. A time-resolved optical study of the same variants [8,9] revealed the presence of a chlorophyll *a* anion with a lifetime that was significantly longer than that of $A_0^-$ irrespective of which branch the mutation was made in. The authors of these studies also concluded that the mutations prevented electron transfer beyond $A_0$, thus extending the lifetime of the $A_{0A}^-$ and $A_{0B}^-$ chlorophyll anions from ~30 ps to several nanoseconds. In contrast, we recently showed that similar variants in *Synechocystis* sp. PCC 6803 caused only partial blockage of electron transfer in the branch carrying the mutation and also altered the rate of electron transfer from the downstream quinone to $F_X$ [10]. Transient EPR, transient absorbance, and molecular dynamics simulations provided evidence that alteration of the $A_1$ to $F_X$ kinetics is due to the formation of an H-bond between the δ-nitrogen of the introduced His and the O1 carbonyl oxygen of the adjacent phylloquinone. This H-bonding arrangement can be seen in Fig. 2, which shows a comparison of the protein-cofactor binding of the $A_{0A}$ chlorophyll and the $A_{1A}$ phylloquinone in the X-ray structure of wild type *T. elongatus* (top) and a structural model of the $M688H_{PsaA}$ variant (bottom).

Differences in the behavior of these PS I variants at low temperature have also been reported between species [11,12]. An electron spin echo envelope modulation (ESEEM) study of whole cells of the wild type and $M668H_{PsaB}$ variant in *Synechocystis* sp. PCC 6803 at 100 K suggested that electron transfer is strongly biased toward the A-branch (A:B branching ratio of <0.2) and signals from the $M688H_{PsaA}$ variant could not be found in whole cells [12]. In contrast, a similar study of the same variants in whole cells of *C. reinhardtii* suggested a branching ratio of 0.42, and a spectrum assigned to $P_{700}^+ A_{1B}^-$ was found if the cells were illuminated before freezing [12]. These results hint at a species-dependent difference in the phenotype of the mutation, but it is difficult to compare the two datasets, which have been collected under different conditions and in different laboratories.

We therefore decided that a systematic study of the behavior of the $M688H_{PsaA}$ and $M668H_{PsaB}$ variants in *C. reinhardtii* and *Synechocystis* sp. PCC 6803 under the same conditions and measured using the same instruments was warranted. Here, we show that there are indeed significant differences between the Met to His variants between the two species. We propose that in *C. reinhardtii*, only the coordination bond to $A_{0A}/A_{0B}$ from the introduced His residue is present whereas in *Synechocystis* sp. PCC 6803, the H-bond to $A_{1A}/A_{1B}$ and the coordination bond to $A_{0A}/A_{0B}$ are present in approximately equal amounts.

## 2. Materials and methods

### 2.1. Construction and growth of the C. reinhardtii $M684H_{PsaA}$ and $M664H_{PsaA}$ variant strains

The $M684H_{PsaA}$ and $M664H_{PsaB}$ mutations were created as described previously [13]. Briefly, the wild type strain CC-125 was used as the recipient for clones containing relevant portions of the PsaA or PsaB genes following site-directed mutagenesis using the QuickChange site-directed mutagenesis kit (Stratagene Inc.) and the aminoglycoside adenyl transferase (*aadA*) gene. Transformants generated by biolistic bombardment were identified by growth on spectinomycin and streptomycin and were brought to homoplasmicity as the concentrations of antibiotics were increased stepwise over several passages. Homoplasmicity was verified by digesting the PCR products of the putative mutation site to specific restriction endonucleases to test for the presence or absence of novel cut sites introduced during site-directed mutagenesis. Cells were harvested and broken in a chilled French press at 3000 psi. Thylakoid membranes were solubilized on ice in darkness with 0.9 % (wt/vol) n-dodecyl-β-D-maltoside at 0.8–1.0 mg Chl $mL^{-1}$ for 20 min and the solubilized fraction was then isolated from the insoluble debris by ultracentrifugation at 65,000 ×*g* for 25 min. Solubilized membrane proteins were laid on sucrose density gradients formed by freeze-thaw of tubes containing 5 mM Tricine–NaOH (pH 8.0), 0.3 M sucrose, 0.3 M betaine, and 0.05% n-dodecyl-β-

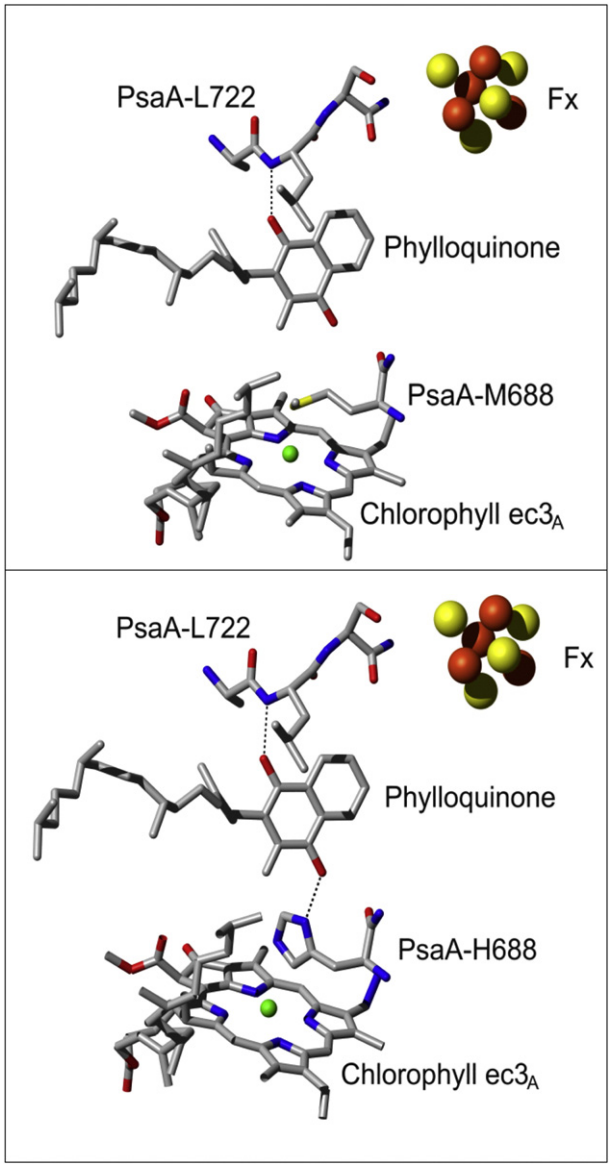


**Fig. 2.** Comparison of the chlorophyll ec3A ($A_{0A}$) and $A_{1A}$ binding region in wild type Photosystem I (top) and the M688$H_{PsaA}$ variant (bottom). The wild type structure is the 2.5-Å resolution X-ray structure of PS I from *T. elongatus* (PDB ID: 1JB0) [2] and the structure of the variant was generated by making a Met to His mutation at residue M688$_{PsaA}$ using DeepView.

D-maltoside. Following a 20-hr centrifugation at 120,000 ×g, the lowest green band was collected and concentrated in buffer containing 5 mM Tricine–NaOH (pH 8.0), 5 mM CaCl2, 5 mM $MgCl_2$ and 0.05% n-dodecyl-β-D-maltoside.

### 2.2. Construction and growth of the Synechocystis sp. PCC 6803 M684H$_{PsaA}$ and M658H$_{PsaB}$ strains

The M684$H_{PsaA}$ and M658$H_{PsaB}$ variants of *Synechocystis* sp. PCC 6803 were generated as described previously [14]. Briefly, plasmids containing the mutations and a chloramphenicol resistance cartridge were constructed using the QuickChange site-directed mutagenesis kit (Stratagene Inc.). The plasmids were then used to transform the pWX3 and pCRTΔB recipient strains. Preparation of thylakoid membranes and isolation of PS I trimers were performed using n-dodecyl-β-D-maltoside according to previously published procedures [15].

### 2.3. Transient EPR spectroscopy

Time/field transient EPR datasets were collected using a modified Bruker ER 200D-SRC spectrometer with either an ER 041 X-MR X-band or an ER 051 QR Q-band microwave bridge. For the X-band datasets, a Flexline ER 4118 X-MD-5W1 dielectric resonator was used at temperatures below 270 K and an ER 4103 TM resonator was employed at room temperature. An ER 5106 QT-W cylindrical resonator was used for the Q-band experiments. Light excitation was achieved using a Continuum Surelite Nd-YAG laser operating at 10 Hz and a wavelength of 532 nm and 4.0 mJ/pulse. The temperature was controlled using an Oxford Instruments CF935 gas flow cryostat. The transient EPR signal was collected in direct-detection mode with a home-built broadband amplifier (bandwidth > 500 MHz) and was digitized using a LeCroy LT322 500 MHz digital oscilloscope and saved on a computer for analysis. Electron donors and mediators (1 mM sodium ascorbate and 50 μM phenazine methosulfate) were added to each sample. For the low temperature experiments, the samples were dark adapted for 20 min on ice and then frozen in the dark to ensure complete reduction of $P_{700}^{+}$ before illumination.

### 2.4. Pulsed EPR experiments

Out-of-phase echo modulation curves were collected at 80 K using a Bruker ELEXSYS E580 spectrometer. The echo was generated using a π/2-τ-π pulse sequence with 8 ns and 16 ns pulses, respectively. The echo intensity was integrated over a 48 ns window centered at the echo maximum. The delay between laser flash and initial microwave pulse was 400 ns. A Continuum Surelite Nd-YAG laser operating at 532 nm, 10 Hz and 3.4 mJ/pulse was used to excite the sample. The resulting echo modulation curves were simulated by taking the powder average,

$$S(\tau,\theta,\phi) = \frac{1}{4\pi}\int_0^{2\pi}\int_0^{\pi} M_x(\tau,\theta,\phi)\sin\theta d\theta d\phi \tag{1}$$

of the out-of-phase magnetization [16–18]:

$$M_x(\tau,\theta,\phi) = \frac{\Delta\omega^2(2J+d)^2}{4\Omega^4}\sin(\Gamma\tau)[1-\cos(2\Omega\tau)]\exp(-\tau/T_2) \tag{2}$$

where $J$ and $d$ are the exchange and dipolar splittings, $\Gamma = 2(J-d)$ is the echo modulation frequency, $\Delta\omega = \frac{\beta B_0}{2\hbar}\left(g_{eff,1}-g_{eff,2}\right)$ and $\Omega = \sqrt{\Delta\omega^2 + (J+d/2)^2}$ is the zero-quantum coherence frequency. $T_2$ is the decay constant of the echo. The g-values and geometry required to calculate $\Delta\omega$ and $d$ have been taken from the recent study by Savitsky et al. [19] for the A-branch radical pair $P_{700}^{+}A_{1A}^{-}$ and from Poluektov et al. [20] for $P_{700}^{+}A_{1B}^{-}$. A value of $T_2 = 600$ ns has been used for all of the *C. reinhardtii* samples. For the *Synechocystis* sp. PCC 6803 samples, decay times of 500, 700 and 900 ns, were used for the M688$H_{PsaA}$, M668$H_{PsaB}$ and wild type samples, respectively. The dipolar splitting, $d$, is related to the coupling constant, $D$, by $d = D(\cos^2\theta - 1/3)$ where $\theta$ is the angle between the vector joining the two spins and the magnetic field. The value of $D$, which is proportional to $1/r^3$, was varied to give the best agreement with the experimental curves and an estimate of the distance between the spins.

### 2.5. Time-resolved optical spectroscopy at 480 nm and 820 nm

Flash-induced absorbance changes were measured at 480 nm and 820 nm using laboratory-built spectrophotometers as described previously [10]. All spectroscopic measurements were performed at room temperature. Data with different time windows were stitched together to span a range from 1 ns to 100 μs (480 nm) and from 1 ns to 100 ms

(820 nm). The data were fit to a multi-exponential decay using the Marquardt least-squares algorithm programmed in Igor Pro v6.3 (Wavemetrics, Portland, OR). The excitation beam was provided by a frequency-doubled (λ = 532 nm), Q-switched Nd:YAG laser (DCR-11; Spectra Physics, Mountain View, CA) operated in the short pulse mode (~3 ns). The output was measured to be 30 mJ per pulse, and was attenuated to 5% by neutral density filters (Edmund Optics, Barrington, NJ).

## 3. Results

### 3.1. Time-resolved optical spectroscopy at 480 nm and 820 nm

Fig. 3 shows optical absorbance difference traces taken at 480 nm for the wild type (top) and the M688H$_{PsaA}$ (middle) and M668H$_{PsaB}$ (bottom) variants. The traces on the left are of PS I complexes from *C. reinhardtii* and those on the right are from *Synechocystis* sp. PCC 6803. The corresponding traces taken at 820 nm are shown in Fig. 4. The absorbance change at 480 nm is the result of an electrochromic band shift of pigments near the quinone when it is in the semiquinone anionic state [21]. The decay of this absorbance change corresponds to forward electron transfer from $A_{1A}^-$ or $A_{1B}^-$ to $F_X$. A small, long-lived absorbance change from $P_{700}^+$ also contributes to the absorbance change at 480 nm. The absorbance change at 820 nm (Fig. 4) is due to formation of $P_{700}^+$. The decay of this signal results from back electron transfer from the various acceptors (<200 ms kinetic phases) to $P_{700}^+$ or from reduction of $P_{700}^+$ by exogenous reductants (slower kinetic phases). The lifetimes and amplitudes of the fitted kinetic components are indicated in the figures and are summarized in Tables 1, 2, and 3.

#### 3.1.1. PS I complexes from the wild-type

In wild-type samples from *C. reinhardtii*, two kinetic phases with lifetimes of 23.7 ns (1.4 mOD) and 227 ns (1.7 mOD) are present at 480 nm. A residual (1.1 mOD) represents long-lived $P_{700}^+$ that does not decay on the timescale of the measurement. The 23.7 ns and 227 ns components are assigned to electron transfer from $A_{1B}^-$ to $F_X$ and from $A_{1A}^-$ to $F_X$, respectively. If the magnitude of the electrochromic shift at 480 nm produced by formation of $A_{1A}^-$ and $A_{1B}^-$ is identical, then the ratio of electron transfer through the A- and B-sides is nearly equivalent (i.e. 55:45). Similarly, two kinetic phases, with lifetimes of 17.1 ns (0.62 mOD) and 207 ns (1.18 mOD), are present in wild-type samples from *Synechocystis*

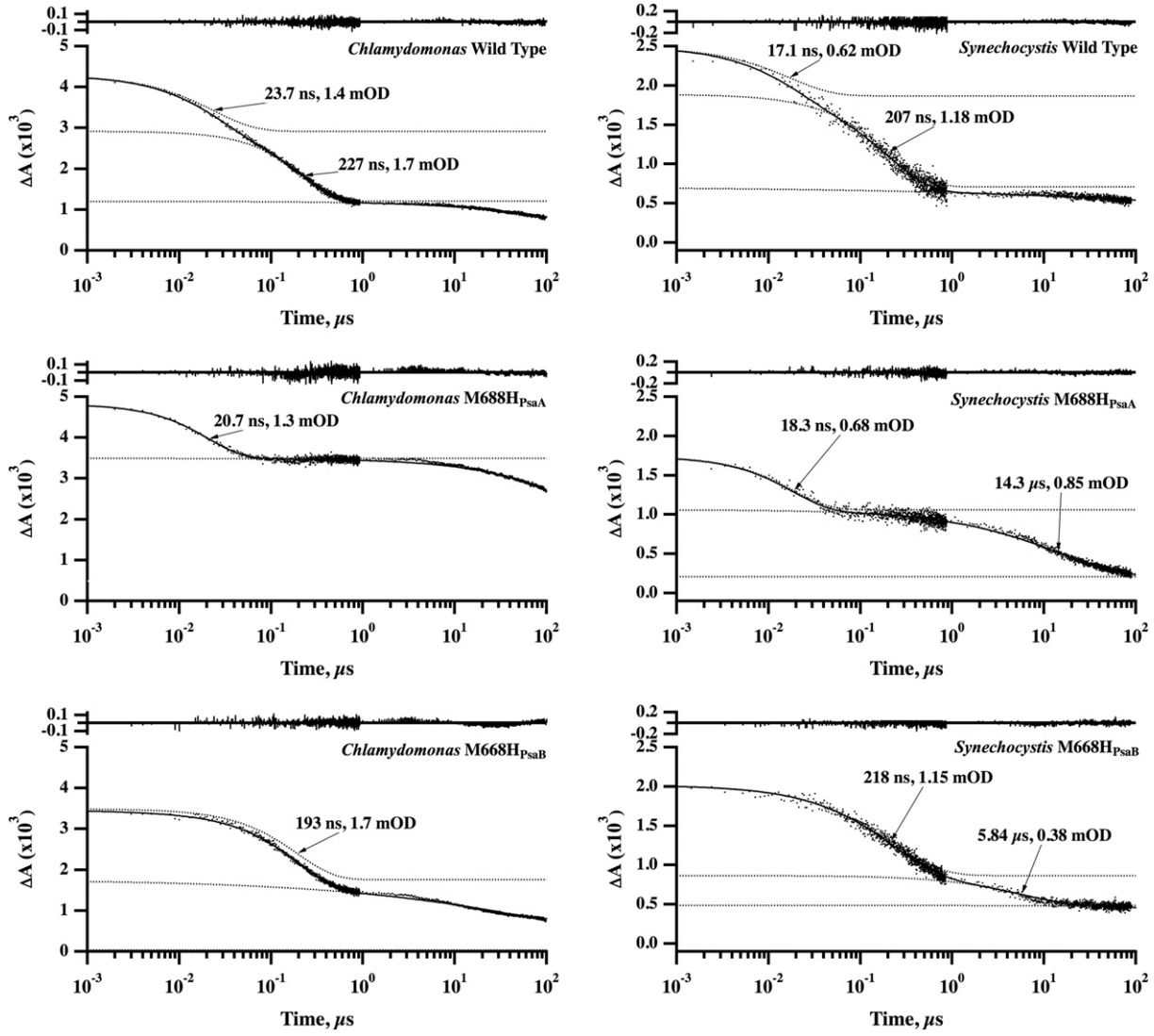


**Fig. 3.** Transient absorbance difference traces at 480 nm for PS I complexes from *C. reinhardtii* (left) and *Synechocystis* sp. PCC 6803 (right). The wild-type, M688H$_{PsaA}$ variant, and M668H$_{PsaB}$ variant are shown in the top, middle, and bottom row of each panel, respectively. The Chl concentration is 100 μg mL$^{-1}$ (*C. reinhardtii*) and 50 μg mL$^{-1}$ (*Synechocystis* sp. PCC 6803). The data sets, which were collected at time windows of 1 ns to 1 μs and from 1 μs to 100 μs, were stitched together to portray multiple kinetic phases on one plot. The absorbance values are plotted on a log scale, and were fitted using a multi-exponential decay. The experimental data are shown as points and the fit is shown as the solid line. The differences between experimental and fit data are plotted as a residual. The data sets were from 64 averages (left) and 16 averages (right). The *Synechocystis* sp. PCC 6803 spectra are reproduced from Ref. [10] with permission.

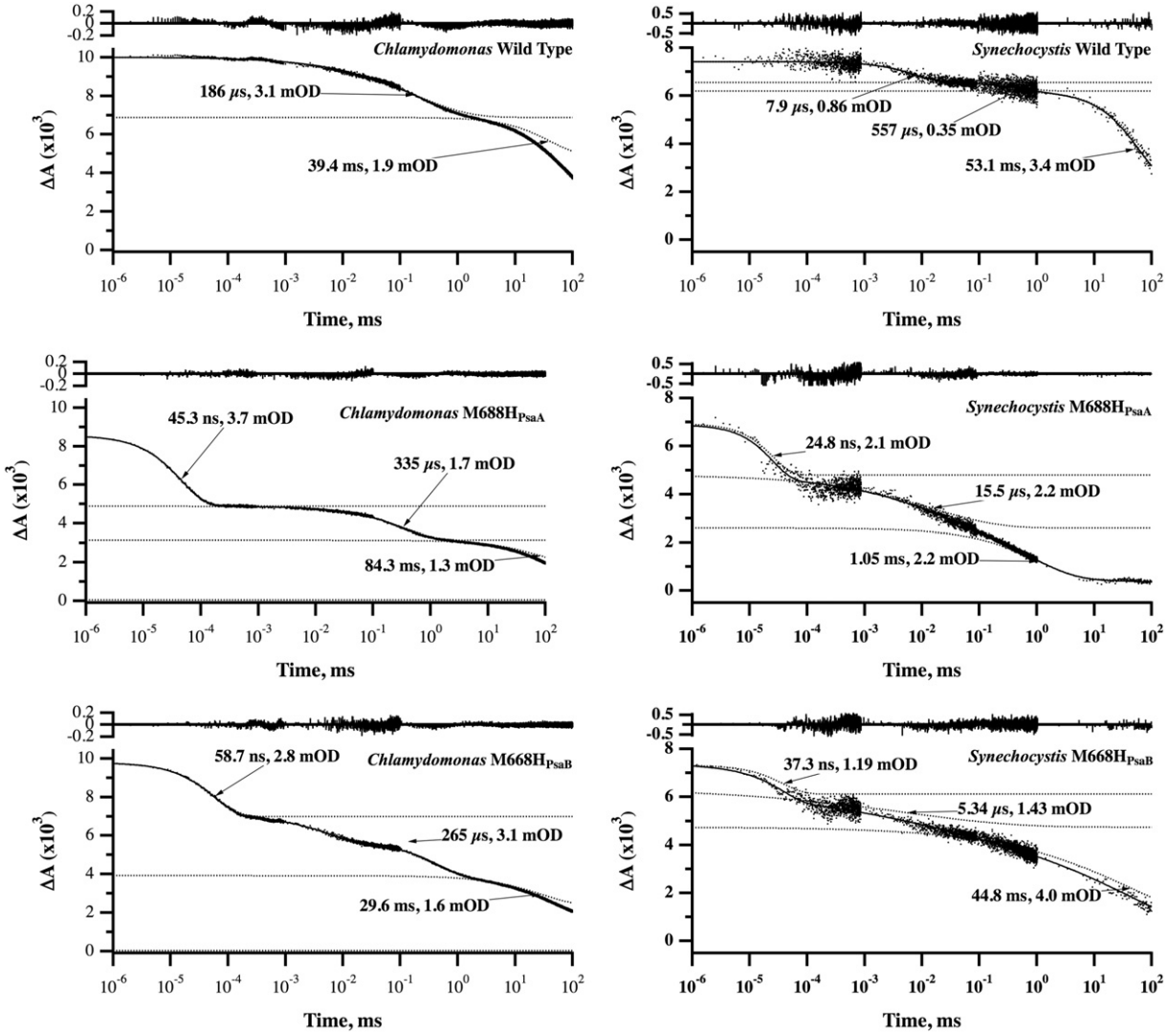


**Fig. 4.** Transient absorbance difference traces at 820 nm for PS I complexes from *C. reinhardtii* (left column) and *Synechocystis* sp. PCC 6803 (right column). The data analysis and conditions are the same as in Fig. 3 except that the chlorophyll concentrations of the *Synechocystis* sp. PCC 6803 was 80 μg mL$^{-1}$. The *Synechocystis* sp. PCC 6803 spectra are reproduced from Ref. [10] with permission.

sp. PCC 6803. Here, the ratio of electron transfer through the A- and B-sides is nearly 2:1 (i.e. 66:34).

At 820 nm, the wild type samples show a kinetic phase with a lifetime of 39.4 ms (1.9 mOD) in *C. reinhardtii* and 53.1 ms (3.4 mOD) in *Synechocystis* sp. PCC 6803 representing the well-characterized charge recombination between $P_{700}^+$ and $[F_A/F_B]^-$. Both samples also show a residual (5.0 mOD in *C. reinhardtii* and 2.8 mOD in *Synechocystis* sp. PCC 6803) from long-lived $P_{700}^+$ that does not decay on the timescale of the measurement. The residual, which is also present in the M688H$_{PsaA}$ and M668H$_{PsaB}$ variants, represents electron donation from DPIP to $P_{700}^+$ in those PS I complexes in which the electron on $[F_A/F_B]^-$ has been lost to an exogenous acceptor (presumably $O_2$). In *Synechocystis* sp. PCC 6803 minor components with lifetimes of 7.9 μs (0.86 mOD)

**Table 1**
WT lifetimes and amplitudes.

| *C. reinhardtii* | | | *Synechocystis* sp. *PCC 6803* | | |
|---|---|---|---|---|---|
| Lifetime | mOD | Assignment | Lifetime | mOD | Assignment |
| *Wild-type, 480 nm* | | | | | |
| 23.7 ns | 1.40 | $A_{1B}^- \rightarrow F_X$ | 17.1 ns | 0.62 | $A_{1B}^- \rightarrow F_X$ |
| 227 ns | 1.70 | $A_{1A}^- \rightarrow F_X$ | 207 ns | 1.18 | $A_{1A}^- \rightarrow P_{700}^+$ |
| >1 μs | 1.10 | $P_{700}^+$ | >1 μs | 0.68 | $P_{700}^+$ |
| Total | 4.20 | | Total | 2.48 | |
| *Wild-type, 820 nm* | | | | | |
| | | | 7.9 μs | 0.86 | $A_1^- \rightarrow P_{700}^+$ |
| (186 μs) | (3.10) | ($^3$Chl) | 557 μs | 0.35 | $F_X^- \rightarrow P_{700}^+$ |
| 39.4 ms | 1.90 | $[F_A/F_B]^- \rightarrow P_{700}^+$ | 53.1 ms | 3.40 | $[F_A/F_B]^- \rightarrow P_{700}^+$ |
| >100 ms | 5.00 | DCPIP $\rightarrow P_{700}^+$ | >100 ms | 2.80 | DCPIP $\rightarrow P_{700}^+$ |
| Total | 6.90 | | Total | 7.41 | |

**Table 2**
M688H$_{PsaA}$ lifetimes and amplitudes.

| *C. reinhardtii* | | | *Synechocystis* sp. *PCC 6803* | | |
|---|---|---|---|---|---|
| Lifetime | mOD | Assignment | Lifetime | mOD | Assignment |
| *M688H$_{PsaA}$ variant, 480 nm* | | | | | |
| 20.7 ns | 1.30 | $A_{1B}^- \rightarrow F_X$ | 18.3 ns | 0.68 | $A_{1B}^- \rightarrow F_X$ |
| | | | 14.3 μs | 0.85 | $A_{1A}^- \rightarrow P_{700}^+$ |
| >1 μs | 3.40 | $P_{700}^+ + ?$ | >1 μs | 0.17 | $P_{700}^+$ |
| Total | 4.70 | | Total | 1.70 | |
| *M688H$_{PsaA}$ variant, 820 nm* | | | | | |
| 45.3 ns | 3.70 | $A_{0A}^- \rightarrow P_{700}^+$ | 24.8 ns | 2.1 | $A_{0A}^- \rightarrow P_{700}^+$ |
| (335 μs) | (1.70) | $^3$Chl | | | |
| | | | 15.5 μs | 2.2 | $A_{1A}^- \rightarrow P_{700}^+$ |
| 84.3 ms | 1.30 | $[F_A/F_B]^- \rightarrow P_{700}^+$ | 1.05 ms | 2.2 | $[F_A/F_B]^- \rightarrow P_{700}^+$ |
| >100 ms | 1.78 | DCPIP $\rightarrow P_{700}^+$ | >100 ms | 0.48 | DCPIP $\rightarrow P_{700}^+$ |
| *Total* | 6.78 | | *Total* | 6.98 | |

**Table 3**
M668H$_{PsaB}$ lifetimes and amplitudes.

| *C. reinhardtii* | | | *Synechocystis* sp. *PCC 6803* | | |
|---|---|---|---|---|---|
| Lifetime | mOD | Assignment | Lifetime | mOD | Assignment |
| *M668H$_{PsaB}$ variant, 480 nm* | | | | | |
| 193 ns | 1.70 | $A_{1A}^{-} \rightarrow F_X$ | 218 ns | 1.15 | $A_{1A}^{-} \rightarrow F_X$ |
| | | | 5.84 μs | 0.38 | $A_{1B}^{-} \rightarrow P_{700}^{+}$ |
| >1 μs | 1.80 | $P_{700}^{+}$ | >1 μs | 0.48 | $P_{700}^{+}$ |
| Total | 3.30 | | Total | 2.01 | |
| *M668H$_{PsaB}$ variant, 820 nm* | | | | | |
| 58.7 ns | 2.80 | $A_{0B}^{-} \rightarrow P_{700}^{+}$ | 37.3 ns | 1.19 | $A_{0B}^{-} \rightarrow P_{700}^{+}$ |
| (265 μs) | (3.10) | $^3$Chl | | | |
| | | | 5.34 μs | 1.43 | $A_{1B}^{-} \rightarrow P_{700}^{+}$ |
| 29.6 ms | 1.60 | $[F_A/F_B]^{-} \rightarrow P_{700}^{+}$ | 44.8 ms | 4.00 | $[F_A/F_B]^{-} \rightarrow P_{700}^{+}$ |
| >100 ms | 2.33 | DCPIP → $P_{700}^{+}$ | >100 ms | 0.71 | DCPIP → $P_{700}^{+}$ |
| Total | 6.73 | | Total | 7.33 | |

and 557 μs (0.35 mOD) represent the backreaction from $A_1^-$ and $F_X^-$ in PS I complexes in which the iron-sulfur clusters have become non-functional. In *C. reinhardtii* these phases are not present but a 186 μs component is seen that does not match any known backreaction in PS I. Similar components are present in both the M688H$_{PsaA}$ (335 μs, 1.7 mOD) and the M668H$_{PsaB}$ (265 μs, 3.1 mOD) samples from *C. reinhardtii*. These kinetic phases are probably due to triplet states from antenna pigments that are unable to transfer their excitation energy to $P_{700}$. These data are summarized in Table 1.

The presence of Chl triplets in the *C. reinhardtii* sample is supported by low temperature transient EPR spectroscopy (see Fig. S1, supporting information). The spectrum, spanning ~60 mT with the polarization pattern EEEAAA (E = emission, A = absorption), is characteristic of a Chl triplet state populated by intersystem crossing. Members of the *Viridiplantae* (plants and green algae) contain additional light-harvesting complexes (LHC), such as LHCI for PS I and LHCII for PS II, to increase the optical cross-section of the two photosystems [22]. LHCI associates tightly and usually co-purifies with PS I. Thus, the Chl triplet spectrum observed in the *C. reinhardtii* sample is probably due to Chl molecules associated with LHCI that are unable to transfer their excitation energy transfer PS I and hence relax via intersystem crossing to the triplet state.

Note that in Fig. S1, no contribution from a Chl triplet is present in the EPR spectrum of wild-type PS I from *Synechocystis* sp. PCC 6803. This agrees with the finding that no kinetic phases in the hundreds-of-microseconds time range are observed by time-resolved optical spectroscopy in this sample. If we neglect the 3.1 mOD absorbance change from the 186 μs component in the wild-type *C. reinhardtii* sample, the total OD at the onset of the flash is 6.9 mOD, which is equivalent to 0.863 μM in $P_{700}$ (100 μg Chl mL$^{-1}$), assuming an extinction coefficient of 8,000 M$^{-1}$ cm$^{-1}$ for $P_{700}$ at 820 nm. This corresponds to 130 Chl/$P_{700}$, which indicates the retention of a population of LHCI with PS I. Indeed, the absence in *C. reinhartdii* of the 8 μs and 0.5 ms kinetic phases that arise from recombination from $A_{1A}^-$ and $F_X^-$ in the *Synechocystis* sp. PCC 6803 sample is consistent with a less harsh treatment of the algal PS I sample, and this may explain the partial retention of LHCI.

### 3.1.2. PS I complexes from the M688H$_{PsaA}$ variant

In the M688H$_{PsaA}$ variant from *C. reinhardtii*, only the B-side kinetic phase, with a lifetime of 20.7 ns (1.3 mOD), is observed at 480 nm on the timescale of the measurement. Its lifetime and amplitude are similar to the 23.7 ns phase in the wild-type. Note that the ~200 ns phase due to A-side electron transfer is completely missing. The residual (3.6 mOD) is due to $P_{700}^+$ and to an intersystem crossing Chl triplet, both of which absorb at this wavelength.

At 820 nm, three kinetic phases, with lifetimes (and amplitudes) of 45 ns (3.7 mOD), 335 μs (1.7 mOD) and 84 ms (3.1 mOD) were resolved in the M688H$_{PsaA}$ variant from *C. reinhardtii*. The 45 ns and 84 ms decay phases are assigned to charge recombination of $P_{700}^+ A_0^-$ and $P_{700}^+ [F_A/F_B]^-$, respectively. Similar to the wild-type, the 335 μs phase is assigned to triplets from antenna Chl molecules associated with LHCI. If the 1.7 mOD absorbance change from this kinetic phase is neglected, the amplitude of the absorbance change at the onset of the flash is 6.78 mOD, which is similar to the amplitude of the total absorbance change in the wild-type sample (7.41 mOD). This indicates that there is no loss in quantum efficiency of charge separation in the M688H$_{PsaA}$ variant, in agreement with a previous study [10].

There are two differences of note when one compares the relevant data from the same variant in *Synechocystis* sp. PCC 6803, First, there is a new ~15 μs phase in the 480 nm decay, which is assigned to recombination of $P_{700}^+ A_{1A}^-$ since it is also observed at 820 nm (Fig. 5). This kinetic phase is absent in the *C. reinhardtii* M688H$_{PsaA}$ variant; at 480 nm, only the ~20 ns phase due to forward electron transfer from $A_{1B}^-$ to $F_X$ and a slow component (lifetime > 1 ms) are seen. Second, the amplitude of the tens-of-ns decay component as a percentage of the total absorbance change at 820 nm is larger in *C. reinhardtii* (55%) than in *Synechocystis* sp. PCC 6803 (30%). A larger amplitude of $P_{700}^+ A_{0A}^-$ recombination is expected in the *C. reinhardtii* M688H$_{PsaA}$ variant since the kinetic phases associated with forward electron transfer from $A_{1A}^-$ to $F_X$ and recombinaton between $A_{1A}^-$ and $P_{700}^+$ are absent. These data are summarized in Table 2.

### 3.1.3. PS I complexes from the M668H$_{PsaB}$ variant

In the M668H$_{PsaB}$ variant of *C. reinhardtii*, only the A-side $A_{1A}^-$ to $F_X$ kinetic phase, with a lifetime of 193 ns (1.7 mOD), is observed at 480 nm on the timescale of the measurement. Its lifetime and amplitude are similar to the 227 ns phase in the wild-type. Note that the ~20 ns phase assigned to B-side electron transfer is completely missing. The residual (1.8 mOD) is due to $P_{700}^+$ and the intersystem crossing Chl triplet.

At 820 nm, three kinetic phases, with lifetimes and amplitudes of 58.7 ns (2.8 mOD), 265 μs (3.1 mOD), and 29.6 ms (1.6 mOD) are resolved in the M668H$_{PsaB}$ variant from *C. reinhardtii*. (A four-component fitting splits the 265 μs component into a 5.1 μs (1.3 mOD) and a 450 μs (1.8 mOD) component, but it is not clear if this distinction is meaningful.) The ~59 ns and ~30 ms decay phases are assigned to charge recombination of $P_{700}^+ A_0^-$ and $P_{700}^+ [F_A/F_B]^-$, respectively. Similar to the wild-type, the 265 μs phase is assigned to triplets from antenna Chl molecules in LHCI. If the 3.05 mOD absorbance change from this kinetic phase is neglected, the amplitude of the absorbance change at the onset of the flash is 6.73 mOD, which is nearly identical to the amplitude of the total absorbance change in the wild-type sample (6.90 mOD). This indicates that there is also no loss in quantum efficiency of charge separation in the M668H$_{PsaB}$ variant, in agreement with a previous study [10].

There are again two differences of note when one compares the relevant data from the same variant in *Synechocystis* sp. PCC 6803. First, there is a new ~5 μs phase in the 480 nm decay, which is assigned to recombination between $P_{700}^+$ and $A_{1B}^-$ since it is also observed at 820 nm (Fig. 5). This kinetic phase is absent in the *C. reinhardtii* M668H$_{PsaB}$ variant; at 480 nm, only the ~200 ns phase due to forward electron transfer from $A_{1A}^-$ to $F_X$ and a slow component (lifetime > 1 ms) are seen. Second, the amplitude of the tens-of-ns kinetic phase as a percentage of the total absorbance change at 820 nm is larger in *C. reinhardtii* (41%) than in *Synechocystis* sp. PCC 6803 (12%), consistent with the conclusion that there is no forward or reverse electron transfer involving $A_{1B}^-$ in the *C. reinhardtii* M668H$_{PsaB}$ variant and hence a larger amount of $P_{700}^+ A_{0B}^-$ recombination occurs. These data are summarized in Table 3.

Taken together, the transient absorbance data indicate that in *C. reinhardtii*, the substitution of Met by a His residue prevents electron beyond the $A_0$ chlorophyll in the branch carrying the mutation, leaving electron transfer in the branch without the mutation unaffected. The situation in *Synechocystis* sp. PCC 6803 is different. Electron transfer from $A_{0A}^-$ to $A_{1A}$ or from $A_{0B}^-$ to $A_{1B}$ can occur in the presence of the His residue in about 50% of the PS I complexes; however, in this fraction, further

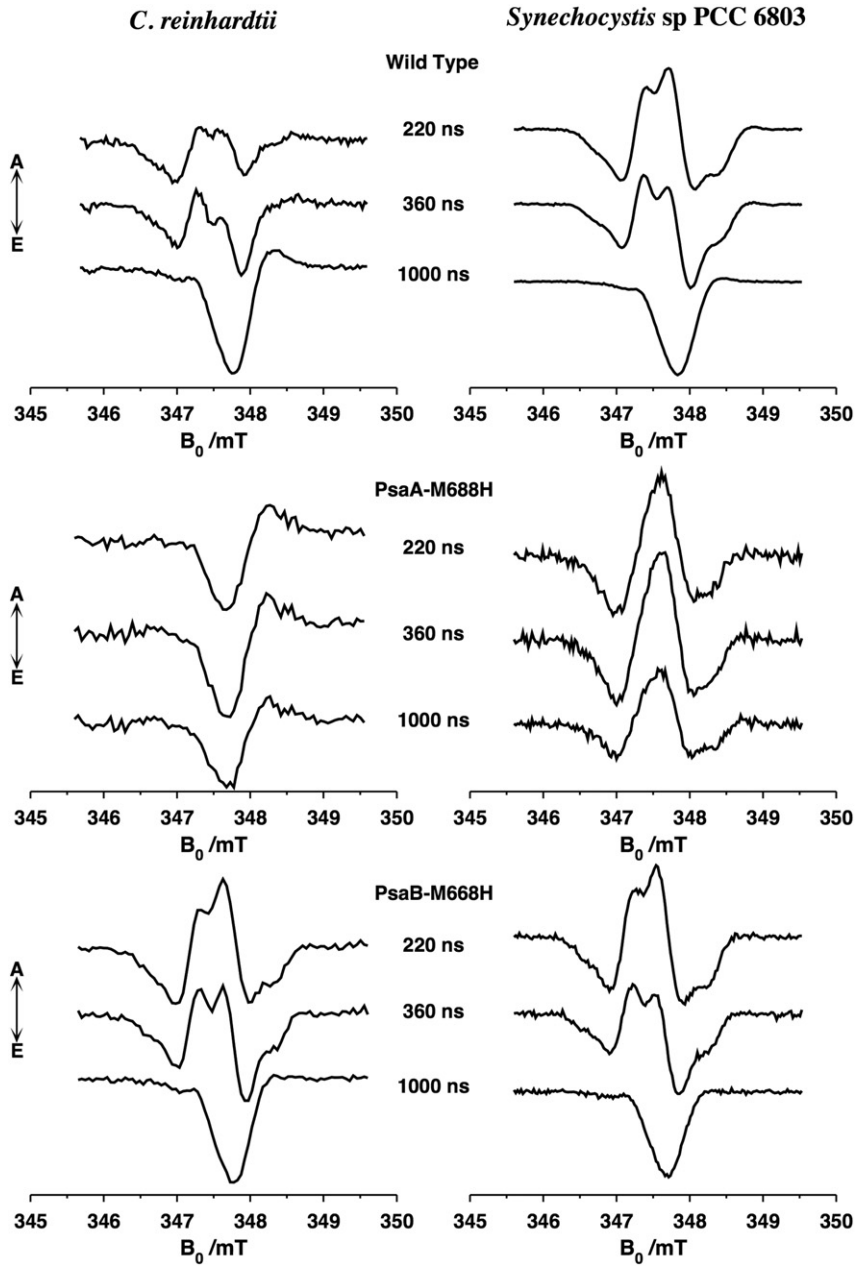


**Fig. 5.** Spin-polarized transient EPR spectra of the $P_{700}^{+}A_1^{-}$ radical pair in *C. reinhardtii* (left) and *Synechocystis* sp. PCC 6803 (right) at room temperature. The wild-type, M688$H_{PsaA}$ variant, and M668$H_{PsaB}$ variant are shown in the top, middle, and bottom row, respectively. Spectra are shown at 220 ns, 360 ns, and 1000 ns after the laser flash. The *Synechocystis* sp. PCC 6803 spectra are reproduced from Ref. [10] with permission.

forward electron transfer from $A_{1A}^{-}$ or $A_{1B}^{-}$ to $F_X$ in the affected branch is blocked.

### 3.2. Room temperature spin-polarized transient EPR spectroscopy

Fig. 5 shows room temperature transient EPR data for the wild type (top), M688$H_{PsaA}$ variant (middle) and the M668$H_{PsaB}$ variant (bottom). The results for *C. reinhardtii* are displayed on the left and those for *Synechocystis* sp. PCC 6803 are on the right; spectra taken at 220 ns, 360 ns and 1000 ns after the laser flash are shown. For the wild type samples, the spectrum at 1000 ns is the almost purely emissive pattern of $P_{700}^{+}$ $(FeS)^{-}$. At 200 ns, the spectrum is a mixture of this pattern and the E/A/E (E for emission and A for absorption) pattern from $P_{700}^{+}$ $A_{1A}^{-}$. The latter decays due to forward electron transfer from $A_{1A}^{-}$ to $F_X$. Fits of the kinetic traces (not shown) give lifetimes of 240 ± 20 ns and 220 ± 20 ns for this event in *Synechocystis* sp. PCC 6803 and *C. reinhardtii*, respectively. The signal of $P_{700}^{+}$ $(FeS)^{-}$ decays with a lifetime of 2 μs in both samples as a result of $T_1$ and $T_2$ spin relaxation. Electron transfer from $A_{1B}^{-}$ to $F_X$ is not resolved kinetically by transient EPR, but it results in a contribution from $P_{700}^{+}$ $(FeS)^{-}$ that is present at early time. Comparison of the spectra of the wild type samples of the two species at 220 ns (Fig. 5, top panels) shows that the central absorptive feature is much weaker in the *C. reinhardtii* sample as a result of a significantly larger contribution from $P_{700}^{+}$ $(FeS)^{-}$. Previous analyses of the room temperature transient EPR data [5,23], give estimates of ~40% B-branch electron transfer in *C. reinhardtii* and <20% B-branch electron transfer in *Synechocystis* sp. PCC 6803. The spectra of the wild-type samples at 1000 ns also show slight differences in the two species, with a larger absorptive contribution on the high field side of the *C. reinhardtii* spectrum. The polarization pattern in this time window

is the $P_{700}^{+}$ contribution to $P_{700}^{+}(FeS)^{-}$ and the primarily emissive polarization arises because of singlet-triplet mixing that has occurred in the precursor radical pairs $P_{700}^{+}A_{1A}^{-}$ and $P_{700}^{+}A_{1B}^{-}$ [24]. The lifetime of $P_{700}^{+}A_{1B}^{-}$ is shorter than that of $P_{700}^{+}A_{1A}^{-}$, hence the amount of net emissive polarization generated by B-branch electron transfer is less. The amount of net polarization is the difference in the intensities of the absorptive and emissive parts of the spectrum. Thus, the fact that the absorptive part of the spectrum at 1000 ns is stronger for the wild type *C. reinhardtii* sample compared to that for wild type *Synechocystis* sp. PCC 6803 (Fig. 5) means it has less net polarization, which is also consistent with a larger amount of B-branch transfer in *C. reinhardtii*.

In the bottom panels of Fig. 5, the corresponding spectra for the $M668H_{PsaB}$ variants are shown. The spectra from the two species are virtually identical at each time point. In both cases, the contribution from $P_{700}^{+}(FeS)^{-}$ to the spectrum at 200 ns is smaller than in the wild type. However, the difference between the wild type spectrum and the $M668H_{PsaB}$ spectrum is greater in *C. reinhardtii* than in *Synechocystis* sp. PCC 6803, in keeping with the greater amount of B-branch electron transfer. At late time, the spectrum is almost purely emissive in both samples, as expected when $P_{700}^{+}(FeS)^{-}$ is formed only from A-branch electron transfer. Thus, the effect of B-side electron transfer in the early TR-EPR spectrum is eliminated in the $M668H_{PsaB}$ variant, but this effect is most obvious in the case of *C. reinhardtii* PS I, which utilizes the B-side to a greater extent.

In contrast to the relatively subtle differences in the wild type spectra, the species-dependent differences of the $M688H_{PsaA}$ variants are striking (Fig. 5, middle). In *Synechocystis* sp. PCC 6803, an E/A/E pattern due to $P_{700}^{+}A_{1A}^{-}$ is seen, while in *C. reinhardtii* only the predominantly emissive spectrum of $P_{700}^{+}(FeS)^{-}$ is seen. In both cases, no evolution of the pattern due to electron transfer occurs, and the signal decays as a result of spin relaxation with a lifetime of ~1 μs in *Synechocystis* sp. PCC 6803 and ~2 μs in *C. reinhardtii*. In *Synechocystis* sp. PCC 6803, the E/A/E pattern lacks the prominent shoulder on the central absorptive peak and less prominent features on the two emissive troughs due to hyperfine coupling with the protons of the methyl substituent at the 2-position of the phylloquinone headgroup. In a previous study, we have argued that the difference in the hyperfine structure is the result of H-bonding between the δ-nitrogen of $H688_{PsaA}$ and the O1 carbonyl oxygen of phylloquinone in the $M688H_{PsaA}$ variant [10]. The optical data suggest that in a fraction of PS I complexes, electron transfer to $A_{1A}$ occurs, but because of the stabilization of the phylloseminoquinone by the H-bond, and a correspondingly higher reduction potential for the quinone/semiquinone redox pair, electron transfer to $F_X$ is unfavorable. In another fraction, electron transfer past $A_{0A}$ is blocked. The EPR data in Fig. 5 suggest that the situation in *C. reinhardtii* is different. Here, there is no evidence for a contribution from $P_{700}^{+}A_{1A}^{-}$, indicating that electron transfer past the $A_{0A}$ is completely blocked. The optical data show that the backreaction from of $P_{700}^{+}A_{0A}^{-}$ occurs with a lifetime of ~30 ns, which is below the time resolution of the EPR spectrometer. Thus, only the spectrum due to $P_{700}^{+}(FeS)^{-}$ arising from B-branch electron transfer is seen. In agreement with this interpretation, the difference in the amplitudes of the absorptive and emissive parts of the spectrum at 1000 ns is smaller in the $M688H_{PsaA}$ sample than in the wild type. As discussed above, the shorter lifetime of $P_{700}^{+}A_{1B}^{-}$ compared to $P_{700}^{+}A_{1A}^{-}$ means that there is less singlet-triplet mixing during B-branch electron transfer hence less net polarization is expected in the $P_{700}^{+}(FeS)^{-}$ spectrum from the $M688H_{PsaA}$ variant.

### 3.3. Low temperature transient EPR spectra

Fig. 6 shows a comparison of X-band transient EPR spectra of all of the PS I samples taken at 80 K. Previous studies have shown that at

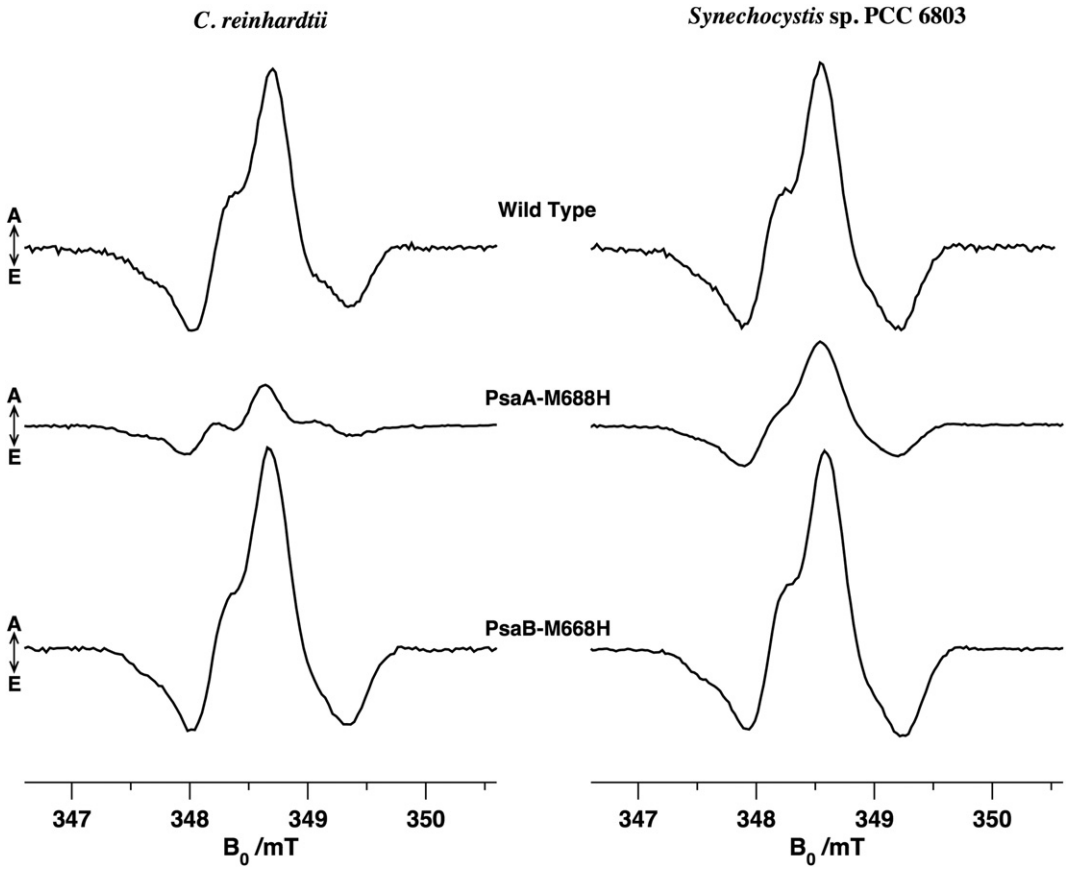


**Fig. 6.** Spin-polarized transient EPR spectra of the $P_{700}^{+}A_{1}^{-}$ radical pair in *C. reinhardtii* (left) and *Synechocystis* sp. PCC 6803 (right) at 80 K. The wild-type, $M688H_{PsaA}$ variant, and $M668H_{PsaB}$ variant are shown in the top, middle, and bottom row, respectively. The spectra were extracted from the time/field datasets in a time window centered at 2.2 μs after the laser flash.

this temperature, several fractions are present in wild type PS I with different behavior following flash excitation, [25–27]. Transient absorbance data show that $P_{700}^{+}$ decays with lifetimes of ~500 μs and ~2 ms [26]. The latter phase can also be seen by time-resolved EPR and can be assigned unambiguously to recombination of $P_{700}^{+}A_1^{-}$. Point mutation studies have shown that only the A-branch radical pair is observed at cryogenic temperatures [28–30]. A small fraction of centers undergo back reaction from the FeS clusters with lifetimes of ~200 ms and several seconds. Irreversible electron transfer between $P_{700}$ and $F_A/F_B$ also takes place. Repeated flashes or steady-state illumination leads to accumulation of $P_{700}^{+}[F_A/F_B]^{-}$ in about 50% of the centers, and this state remains stable indefinitely at this temperature. The transient EPR spectra shown in Fig. 6 arise from the fraction of PS I complexes in which reversible electron transfer to $A_{1A}$ occurs. The A-branch mutation causes a significant reduction in the intensity of the 80 K transient EPR spectrum compared to the wild type, as would be expected since the room temperature data indicate that A-branch electron transfer is either partially or completely blocked in the $M668H_{PsaA}$ variants. In contrast, the B-branch mutations cause little change in signal amplitude.

Closer inspection of the spectra of $M688H_{PsaA}$ variants shows that they are not the same in the two species. In particular, the low-field shoulder on the central absorption peak is different. Compared to the wild-type, it is less pronounced in the *Synechocystis* sp. PCC 6803 $M688H_{PsaA}$ variant, while it is much more pronounced in the *C. reinhardtii* $M688H_{PsaA}$ variant. This feature is due to hyperfine coupling to the protons of the 2-methyl group of the phylloquinone headgroup [14,31,32]. In the wild type, the fact that the O1 oxygen is H-bonded to the protein while the O4 oxygen is not, leads to high spin density adjacent to the methyl group and hence a pronounced hyperfine splitting [31]. Molecular dynamics simulations of the $M688H_{PsaA}$ variant suggest that the His side chain can form an H-bond to the O4 carbonyl oxygen of phylloquinone [10]. The change in the H-bonding is expected to result in a more symmetric spin density distribution and less pronounced methyl hyperfine coupling than in the corresponding wild-type spectrum, as is observed for the $M688H_{PsaA}$ variant in *Synechocystis* sp. PCC 6803 at both 80 K (Fig. 7) and room temperature (Fig. 3). In contrast, in *C. reinhardtii* the hyperfine couplings in the $M688H_{PsaA}$ variant are stronger than in the wild-type.

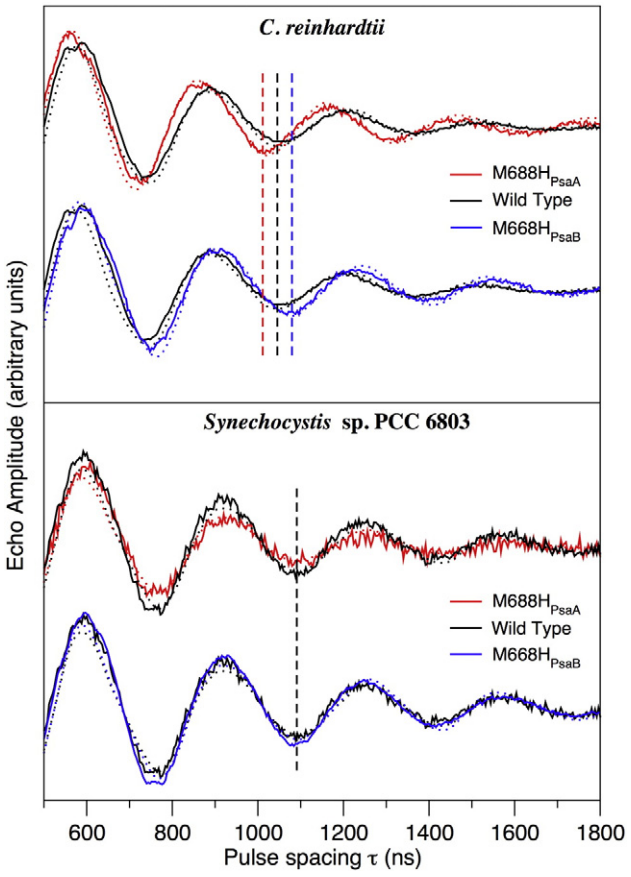


**Fig. 7.** Out-of-phase echo modulation curves at 80 K. Black: wild type, red: $M688H_{PsaA}$, blue: $M668H_{PsaB}$. Solid curves: experimental data, dotted curves: simulations. The vertical dashed lines show the position of the trough near $\tau = 1100$ ns. Notice that the position of this feature is identical for all three samples of *Synechocystis* sp. PCC 6803 PS I but is different for the three *C. reinhardtii* samples.

There are also differences between the samples in the emissive feature on the high-field end of the spectra. The spectra of the wild-type and $M668H_{PsaB}$ variant in both *Synechocystis* sp. PCC 6803 and *C. reinhardtii* are virtually identical and the high-field emission has about the same intensity as the low-field emission. In the *C. reinhardtii* wild-type spectrum the high-field emission is significantly weaker, and it is extremely weak in the *C. reinhardtii* $M688H_{PsaA}$ variant. These differences can be seen more clearly in the overlay of the spectra shown in Fig. S2 in the supporting information.

In light of the room temperature optical and EPR data, which show that the kinetic phases and spectral features associated with A-branch electron transfer are completely absent in the *C. reinhardtii* $M688H_{PsaA}$ variant, we postulate that the low-temperature transient EPR spectrum of this variant is due to the B-branch radical pair $P_{700}^{+}A_{1B}^{-}$. In contrast, the room temperature data suggest that A-branch electron transfer is only partially blocked in the *Synechocystis* sp. PCC 6803 $M688H_{PsaA}$ variant, and the less pronounced hyperfine coupling suggest that the spectrum is due to the $P_{700}^{+}A_{1A}^{-}$ radical pair in which the His imidazole is H-bonded to $A_{1A}$. Furthermore, the difference in the high-field emissive features in the two wild-type spectra implies that there may be a contribution from the B-branch radical pair in the spectrum of wild type *C. reinhardtii*. This is in line with two recent studies, which suggest that at low temperature a larger amount of B-branch electron transfer occurs in *C. reinhardtii* than in cyanobacterial PS I [11,12].

### 3.4. Out-of-phase ESEEM experiments

The contribution from the $P_{700}^{+}A_{1A}^{-}$ and $P_{700}^{+}A_{1B}^{-}$ radical pairs to the low temperature spectra in Fig. 6 can be probed by out-of-phase electron spin echo envelope modulation (OOP-ESEEM) experiments. Because the electron spin density on $P_{700}^{+}$ is localized predominantly on chlorophyll ec1B of $P_{700}$ [33], the distance between the electron spins in the $P_{700}^{+}A_{1A}^{-}$ and $P_{700}^{+}A_{1B}^{-}$ radicals pairs are different [19,34]. This difference is observable as different modulation frequencies in OOP-ESEEM experiments [34]. Fig. 7 shows a comparison of the OOP-ESEEM traces for the various samples from *Synechocystis* sp. PCC 6803 and *C. reinhardtii*. The position of the trough near $\tau = 1100$ ns can be used as a qualitative marker for the modulation frequency and the dashed vertical lines in Fig. 7 indicate the position of this trough. For the three *Synechocystis* sp. PCC 6803 samples the modulation frequency is the same, while for the three *C. reinhardtii* samples the position of the trough changes, indicating that the mutations cause a change in the modulation frequency. The distance between the two electron spins in the $P_{700}^{+}A_{1A}^{-}$ and $P_{700}^{+}A_{1B}^{-}$ radicals pairs have been estimated to be 26.0 Å and 25.3 Å, respectively. [19] Thus, a larger dipolar coupling, and consequently higher modulation frequency is expected for the B-branch radical pair. Consistent with the hypothesis that the low temperature transient EPR spectrum of the $M688H_{PsaA}$ variant in *C. reinhardtii* is due to the B-branch radical pair, the position of the trough around $\tau =$ 1100 ns indicated by the dashed vertical red line in Fig. 7 is shifted to the left in the variant, indicating a higher modulation frequency. In contrast, the curves from the *C. reinhardtii* $M668H_{PsaB}$ sample and the three *Synechocystis* sp. PCC 6803 samples all have essentially the same frequency, consistent with the dominance of the A-branch radical pair at 80 K. The position of the trough for the *C. reinhardtii* wild-type sample

indicated by the vertical dashed black line in the upper part of Fig. 7 is intermediate, suggesting that the presence of both radical pairs.

The dotted curves in Fig. 7 are simulations of the ESEEM data. The geometric parameters obtained from an analysis of W-band data of the A-branch [19] and B-branch [20] radical pairs have been used. The dipolar coupling was adjusted to give the best agreement with the experimental traces and the exchange coupling was held fixed at J = 1 μT. For the three *Synechocystis* sp. PCC 6803 samples, a value of D = −0.165 ± 0.02 mT is obtained for the dipolar coupling constant, which corresponds to a distance of 25.7 ± 0.3 Å between the spins. This value is within error the same as found previously from the analysis of X-band data from cyanobacterial PS I samples [12,18,35,36] and corresponds to the A-branch radical pair [14,19,28,30]. For the *C. reinhardtii* M668$H_{PsaB}$ variant, the fit gave D = −0.168 ± 0.02 mT, which is within error the same as for the *Synechocystis* sp. PCC 6803 samples. However, for the *C. reinhardtii* M688$H_{PsaA}$ variant, the dipolar coupling is larger (D = −0.172 ± 0.02 mT) corresponding to a slightly shorter distance of 25.3 ± 0.3 Å. The modulation curve for the wild-type *C. reinhardtii* sample can be simulated as a weighted sum of the simulations from the M668$H_{PsaB}$ and M688$H_{PsaA}$ variants at a ratio of 3:2. The difference of 0.4 Å in the distances for the two *C. reinhardtii* variants is close to the value of 0.6 Å estimated for the difference in the interspin distances for the A- and B-branch radical pairs [19]. Thus, the OOP-ESEEM data suggest that in *C. reinhardtii*, the low temperature EPR signals are due to the A-branch radical pair in the M668$H_{PsaB}$ variant and to the B-branch radical pair in the M688$H_{PsaA}$ variant and a 3:2 mixture of these two species in the wild-type. This is in line with previous studies that have shown only the A-branch radical pair contributes to the OOPE modulation in wild type *Synechocystis* sp. PCC 6803 samples [19] but that both A- and B-branch radical pairs contribute to the low temperature spectra and OOPE traces from *C. rheinhardtii* wild type samples. [11,12,34]

## 4. Discussion

The experimental results described here paint the following picture of the effect of the Met to His mutations in the two species. In *C. reinhardtii*, forward electron transfer from $A_0$ to $A_1$ is blocked in the branch carrying the mutation in all of the PS I complexes. In *Synechocystis* sp. PCC 6803, forward electron transfer from $A_0$ to $A_1$ occurs in the branch carrying the mutation in about half of the PS I complexes and is blocked in the other half. In those PS I complexes in which electron transfer from $A_0$ to $A_1$ occurs, further electron transfer to $F_X$ is blocked. The spin density distribution of $A_1^-$ is also altered in the cyanobacterial variants. Previously, we presented molecular dynamics simulations demonstrating that several conformations of the His side chain are possible [10]. All of the minimum energy conformations calcuated in the simulation show His coordinating the central Mg of ec2, but only a subset of the conformations also have an H-bond between the His δ-nitrogen and the O1 carbonyl of phylloquinone. The behavior of the His variants in the two species can be most easily explained as a difference in the relative amounts of the latter conformer. In *Synechocystis* sp. PCC 6803, it appears that the H-bonded conformer occurs in roughly 50% of PS I complexes, while in *C. reinhardtii* this conformer is not present.

The effect of the mutation in the two variants can be explained by postulating that the substitution of His for Met stabilizes $A_0^-$ so that there is less driving force for forward electron transfer to $A_1$ (Fig. 8). With sufficient stabilization, the rate of forward transfer would become slower than the back reaction rate and the electron on $A_0^-$ would recombine with $P_{700}^+$, forming the triplet state of the latter. The proposed stabilization of $A_0^-$ accounts for both the 25 ns phase in the time-resolved optical studies reported here (Fig. 4) and the spin-polarized EPR spectrum of $^3P_{700}$ reported in Fig. 8 of Ref. [10] which indicates that backreaction from $A_0^-$ occurs. However in the *C. reinhardtii* variants, back reaction from $A_0^-$ occurs in all PS I complexes, while in *Synechocystis* sp. PCC 6803 variants, the block in forward electron transfer from $A_0$ to $A_1$ is only seen in roughly half of the PS I complexes. This difference can be explained by proposing that in *Synechocystis* sp. PCC 6803, His is H-bonded to phylloquinone in the PS I complexes in which electron transfer from $A_0$ to $A_1$ occurs. The H-bonding stabilizes $A_1^-$ (Fig. 8), which results in sufficient driving force to permit $A_0^-$ to $A_1$ electron transfer to occur. The 5 μs and 15 μs decay components observed at both 820 nm and 480 nm that represent charge recombination of $P_{700}^+A_{1B}^-$ and

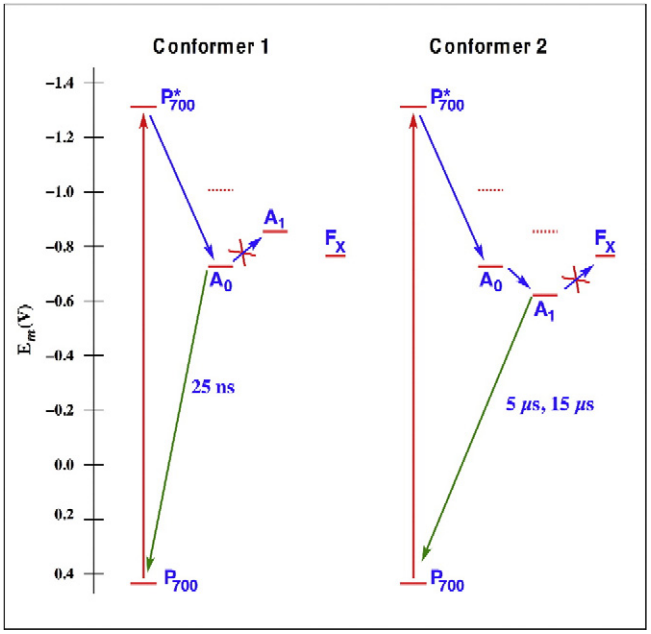


**Fig. 8.** Diagram of the approximate mid-point potentials of the cofactors and backreaction lifetimes in the two proposed conformers of PS I from the Met to His variants. The dashed lines represent the estimate energies of $P_{700}^+A_0^-$ and $P_{700}^+A_1^-$ in wild type PS I. In *C. reinhardtii* only conformer 1 (left) is present, while in *Synechocystis* sp. PCC 6803 both conformers are found in roughly equal amounts.

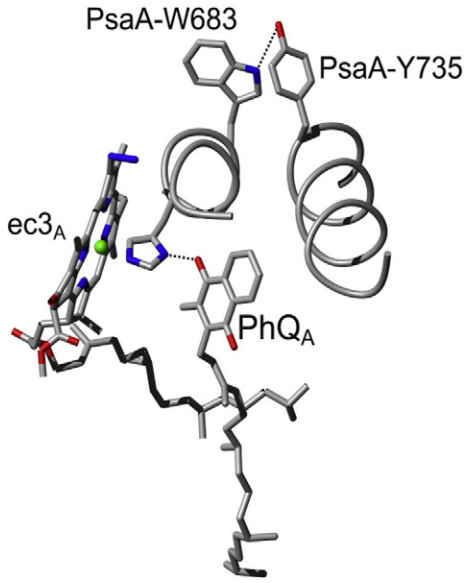


**Fig. 9.** Structural details around the residue W683$_{PsaA}$, which is conserved in *Synechocystis* sp. PCC 6803, but is a Phe residue in *C. reinhardtii*. The figure was constructed from the 2.5-Å resolution X-ray structure of PS I from *T. elongatus* (PDB ID: 1JB0) [2] using molmol [39].

$P_{700}^{+}A_{1A}^{-}$ can be explained by proposing that the stabilization of $A_1^-$ by the H-bond makes forward electron transfer to $F_X$ now unfavorable. The reason for the differing amounts of the two conformers in the two species is not known, but a comparison of the amino acid sequences and cofactor structures of the two species allows some possibilities to be identified.

The amino acid sequences near $M688_{PsaA}$ and $M668_{PsaB}$ are very well conserved between the two species. However, the Trp residues $W683_{PsaA}$ and $W663_{PsaB}$ in *Synechocystis* sp. PCC 6803 are Tyr and Phe, respectively, in *C. reinhardtii*. The X-ray structure shows that in *Synechococcus elongatus* $W683_{PsaA}$ is H-bonded to $Y735_{PsaA}$ as shown Fig. 9. The sequences of *Synechocystis* sp. PCC 6803 and *Thermosynechocystis elongatus* are highly conserved in this region and one can safely assume that this H-bond is also present in the former. However, in *C. reinhardtii* the residue corresponding to $W683_{PsaA}$ is Phe, and hence the H-bond must be absent. It is conceivable that in the absence of this H-bond, the conformation of the surrounding protein in the $M688H_{PsaA}$ variant is altered in such a way that H-bonding between $A_{1A}$ and His $M688H_{PsaA}$ becomes unfavorable or is not allowed due to steric constraints. However, the side chain of the residue at position 683 of PsaA is well removed from position 688 on the opposite face of the helix, which suggests that the influence of any sequence difference at position 683 might be small.

Another difference between the two organisms is the nature of the quinones in PS I. In *Synechocystis* sp. PCC 6803 they are phylloquinone [37] but in *C. reinhardtii* they are 5′-hydroxyphylloquinone [38]. This difference means that the side chain of the quinone in *C. reinhardtii* is more polar than in *Synechocystis* sp. PCC 6803 and it is possible that this difference has an influence on the formation of the H-bond between His and phylloquinone. However, the position of the OH group is rather far from the phylloquinone headgroup and its effect is not expected to be large. Thus, the origin of the species difference remains unclear.

The data presented here are relevant to the discussion of the directionality of electron transfer in PS I and for the reasons of the different rates of $A_1^-$ to $F_X$ in the two branches. In a recent study, the structure of the B-branch radical $P_{700}^{+}A_{1B}^{-}$ was estimated from an analysis of Q-band transient EPR data from the $M688H_{PsaA}$ variant in deuterated whole cells of *C. reinhardtii* [11]. Based on the geometry, it was suggested that the H-bond between $A_{1B}$ and the protein backbone is weakened in the charge-separated state and that the faster rate of $A_1^-$ to $F_X$ electron transfer in the B-branch compared to the A-branch may be due to a lowering of the reduction potential of $A_{1B}$ as a result of the proposed weakening of the H-bond. The data in Fig. 6 do not support this hypothesis. The structure in the spectrum of $P_{700}^{+}A_{1B}^{-}$ in the *C. reinhardtii* $M688H_{PsaA}$ variant in Fig. 6 and the linewidths reported in the literature for $P_{700}^{+}A_{1B}^{-}$ [20] indicate that the hyperfine coupling to the methyl group is stronger in $A_{1B}^{-}$ than in $A_{1A}^{-}$, which implies stronger H-bonding. If the proposed weakening of the H-bond were to occur, the hyperfine coupling would be expected to decrease rather than increase as observed.

Finally, recent EPR studies have provided strong evidence that in PS I from *Synechocystis* sp. PCC 6803, electron transfer at low temperature is very strongly biased toward the A-branch [12,19,25]. The transient EPR spectra (Fig. 6) and OOP-ESEEM curves (Fig. 7) are consistent with this conclusion. However, there are noticeable differences between the *C. reinhardtii* and *Synechocystis* sp. PCC 6803 data, consistent with a contribution from the B-branch radical pair in the latter. The origin of this difference is unclear but it governed by the relative use of the two branches and the heterogeneity in the electron transfer equilibria between the iron-sulfur clusters and the phylloquinones.

## Transparency document

The Transparency document associated with this article can be found, in the online version.

## Acknowledgements

We acknowledge support in the form of a Natural Sciences and Engineering Research Council of Canada (NSERC) Discovery Grant to A.v.d.E., grant MCB-1021725 from the US National Science Foundation to J.H.G., grant DE-FG02-99ER20349 from the U.S. Department of Energy to A.W., grant MCB-1052573 from the U.S. National Science Foundation to K.R, and a post-graduate scholarship (PGS-B) from NSERC to M.D.M

## Appendix A. Supplementary data

Supplementary data to this article can be found online at http://dx.doi.org/10.1016/j.bbabio.2015.01.011.

## References

[1] P. Fromme, P. Jordan, N. Krauß, Structure of photosystem I, Biochim. Biophys. Acta 1507 (2001) 5–31.
[2] P. Jordan, P. Fromme, H.T. Witt, O. Klukas, W. Saenger, N. Krauß, Three dimensional structure of photosystem I at 2.5 Å resolution, Nature 411 (2001) 909–917.
[3] K. Redding, A. van der Est, Directionality of electron transfer in photosystem I, in: J. Golbeck (Ed.), Phototosystem I: The Light-Induced Plastocyanin:Ferredoxin Oxidoreductase, Springer, Dordrecht, 2006, pp. 413–437.
[4] N. Dashdorj, W. Xu, R.O. Cohen, J.H. Golbeck, S. Savikhin, Asymmetric electron transfer in cyanobacterial Photosystem I: charge separation and secondary electron transfer dynamics of mutations near the primary electron acceptor A0, Biophys. J. 88 (2005) 1238–1249.
[5] Y.J. Li, A. van der Est, M.G. Lucas, V.M. Ramesh, F.F. Gu, A. Petrenko, S. Lin, A.N. Webber, F. Rappaport, K. Redding, Directing electron transfer within photosystem I by breaking H-bonds in the cofactor branches, Proc. Natl. Acad. Sci. U. S. A. 103 (2006) 2144–2149.
[6] A.R. Holzwarth, M.G. Muller, C. Slavov, R. Luthra, K. Redding, Ultrafast energy and electron transfer in photosystem I — direct evidence for two-branched electron transfer, Springer Ser. Chem. 88 (2007) 471–473.
[7] W.V. Fairclough, A. Forsyth, M.C. Evans, S.E. Rigby, S. Purton, P. Heathcote, Bidirectional electron transfer in photosystem I: electron transfer on the PsaA side is not essential for phototrophic growth in *Chlamydomonas*, Biochim. Biophys. Acta 1606 (2003) 43–55.
[8] V.M. Ramesh, K. Gibasiewicz, S. Lin, S.E. Bingham, A.N. Webber, Bidirectional electron transfer in photosystem I: accumulation of A(0)(−) in A-side or B-side mutants of the axial ligand to chlorophyll A(0), Biochemistry 43 (2004) 1369–1375.
[9] V.M. Ramesh, K. Gibasiewicz, S. Lin, S.E. Bingham, A.N. Webber, Replacement of the methionine axial ligand to the primary electron acceptor A(0) slows the A(0)(−)reoxidation dynamics in Photosystem I, Biochim. Biophys. Acta 1767 (2007) 151–160.
[10] J. Sun, S. Hao, M. Radle, W. Xu, I. Shelaev, V. Nadtochenko, V. Shuvalov, A. Semenov, H. Gordon, A. van der Est, J. Golbeck, Evidence that histidine forms a coordination bond to the A0A and A0B chlorophylls and a second H-bond to the A1A and A1B phylloquinones in M688HPsaA and M668HPsaB variants of *Synechocystis* sp. PCC 6803, Biochim. Biophys. Acta 1837 (2014) 1362–1375.
[11] T. Berthold, E.D. von Gromoff, S. Santabarbara, P. Stehle, G. Link, O.G. Poluektov, P. Heathcote, C.F. Beck, M.C. Thurnauer, G. Kothe, Exploring the electron transfer pathways in photosystem I by high-time-resolution electron paramagnetic resonance: observation of the B-side radical pair P(700)(+)A(1B)(−) in whole cells of the deuterated green alga *Chlamydomonas reinhardtii* at cryogenic temperatures, J. Am. Chem. Soc. 134 (2012) 5563–5576.
[12] S. Santabarbara, I. Kuprov, O. Poluektov, A. Casal, C.A. Russell, S. Purton, M.C.W. Evans, Directionality of electron-transfer reactions in photosystem I of prokaryotes: universality of the bidirectional electron-transfer model, J. Phys. Chem. B 114 (2010) 15158–15171.
[13] V.M. Ramesh, S.E. Bingham, A.E. Webber, A simple method for chloroplast transformation in *Chlamydomonas reinhardtii*, Methods Mol. Biol. 684 (2011) 313–320.
[14] W. Xu, P. Chitnis, A. Valieva, A. van der Est, Y.N. Pushkar, M. Krzystyniak, C. Teutloff, S.G. Zech, R. Bittl, D. Stehlik, B. Zybailov, G. Shen, J.H. Golbeck, Electron transfer in cyanobacterial photosystem I: I. Physiological and spectroscopic characterization of site-directed mutants in a putative electron transfer pathway from A0 through A1 to FX, J. Biol. Chem. 278 (2003) 27864–27875.
[15] T.W. Johnson, G.Z. Shen, B. Zybailov, D. Kolling, R. Reategui, S. Beauparlant, I.R. Vassiliev, D.A. Bryant, A.D. Jones, J.H. Golbeck, P.R. Chitnis, Recruitment of a foreign quinone into the A(1) site of photosystem I — I. Genetic and physiological characterization of phylloquinone biosynthetic pathway mutants in *Synechocystis* sp PCC 6803, J. Biol. Chem. 275 (2000) 8523–8530.
[16] K. Salikhov, Y.E. Kandrashkin, A.K. Salikhov, Peculiarities of free induction and primary spin echo signals for spin-correlated radical pairs, Appl. Magn. Reson. 1 (1992) 199–216.
[17] J. Tang, M.C. Thurnauer, J.R. Norris, Electron-spin echo envelope modulation due to exchange and dipolar interactions in a spin-correlated radical pair, Chem. Phys. Lett. 219 (1994) 283–290.
[18] R. Bittl, S.G. Zech, Pulsed EPR study of spin-coupled radical pairs in photosynthetic reaction centers: measurement of the distance between $P_{700}^{\cdot+}$ and $A_1^{\cdot-}$ in

photosystem I and between $P_{865}^{\cdot+}$ and $Q_A^{\cdot-}$ in bacterial reaction centers, J. Phys. Chem. B 101 (1997) 1429–1436.
[19] A. Savitsky, J. Niklas, J.H. Golbeck, K. Mobius, W. Lubitz, Orientation resolving dipolar high-field EPR spectroscopy on disordered solids: II. Structure of spin-correlated radical pairs in photosystem I, J. Phys. Chem. B 117 (2013) 11184–11199.
[20] O.G. Poluektov, S.V. Paschenko, L.M. Utschig, K.V. Lakshmi, M.C. Thurnauer, Bidirectional electron transfer in photosystem I: direct evidence from high-frequency time-resolved EPR spectroscopy, J. Am. Chem. Soc. 127 (2005) 11910–11911.
[21] J.A. Bautista, F. Rappaport, M. Guergova-Kuras, R.O. Cohen, J.H. Golbeck, J.Y. Wang, D. Beal, B.A. Diner, Biochemical and biophysical characterization of photosystem I from phytoene desaturase and xi-carotene desaturase deletion mutants of *Synechocystis* sp PCC 6803, J. Biol. Chem. 280 (2005) 20030–20041.
[22] B.R. Green, D.G. Durnford, The chlorophyll–carotenoid proteins of oxygenic photosynthesis, Annu. Rev. Plant Physiol. 47 (1996) 685–714.
[23] Y.E. Kandrashkin, A. van der Est, Electron spin polarization in photosynthetic reaction centres: strategies for extracting structural and functional information, RIKEN Rev. 44 (2002) 124–127.
[24] Y.E. Kandrashkin, K.M. Salikhov, A. van der Est, D. Stehlik, Electron spin polarization in consecutive spin-correlated radical pairs: application to short-lived and long-lived precursors in type 1 photosynthetic reaction centres, Appl. Magn. Reson. 15 (1998) 417–447.
[25] S. Mula, A. Savitsky, K. Mobius, W. Lubitz, J.H. Golbeck, M.D. Mamedov, A.Y. Semenov, A. van der Est, Incorporation of a high potential quinone reveals that electron transfer in Photosystem I becomes highly asymmetric at low temperature, Photochem. Photobiol. Sci. 11 (2012) 946–956.
[26] A. Savitsky, O. Gopta, M. Mamedov, J.H. Golbeck, A. Tikhonov, K. Mobius, A. Semenov, Alteration of the axial Met ligand to electron acceptor A(0) in photosystem I: effect on the generation of $P_{700}^{\cdot+}$ $A_1^{\cdot-}$ $P_{700}^{\cdot+}A_1^{\cdot-}$ radical pairs as studied by W-band transient EPR, Appl. Magn. Reson. 37 (2010) 85–102.
[27] E. Schlodder, K. Falkenberg, M. Gergeleit, K. Brettel, Temperature dependence of forward and reverse electron transfer from A(1)(−), the reduced secondary electron acceptor in photosystem I, Biochemistry 37 (1998) 9466–9476.
[28] W. Xu, P.R. Chitnis, A. Valieva, A. van der Est, K. Brettel, M. Guergova-Kuras, Y.N. Pushkar, S.G. Zech, D. Stehlik, G. Shen, B. Zybailov, J.H. Golbeck, Electron transfer in cyanobacterial photosystem I: II. Determination of forward electron transfer rates of site-directed mutants in a putative electron transfer pathway from A0 through A1 to FX, J. Biol. Chem. 278 (2003) 27876–27887.
[29] S. Purton, D.R. Stevens, I.P. Muhiuddin, M.C.W. Evans, S. Carter, S.E.J. Rigby, P. Heathcote, Site-directed mutagenesis of PsaA residue W693 affects phylloquinone binding and function in the photosystem I reaction center of *Chlamydomonas reinhardtii*, Biochemistry 40 (2001) 2167–2175.
[30] B. Boudreaux, F. MacMillan, C. Teutloff, R. Agalarov, F. Gu, S. Grimaldi, R. Bittl, K. Brettel, K. Redding, Mutations in both sides of the Photosystem I reaction center identify the phylloquinone observed by electron paramagnetic resonance spectroscopy, J. Biol. Chem. 276 (2001) 37299–37306.
[31] J. Niklas, B. Epel, M.L. Antonkine, S. Sinnecker, M.E. Pandelia, W. Lubitz, Electronic structure of the quinone radical anion $A_1^{\cdot-}$ of photosystem I investigated by advanced pulse EPR and ENDOR techniques, J. Phys. Chem. B 113 (2009) 10367–10379.
[32] S. Mula, M.D. McConnell, A. Ching, N. Zhao, H.L. Gordon, G. Hastings, K.E. Redding, A. van der Est, Introduction of a hydrogen bond between phylloquinone PhQ(A) and a threonine side-chain OH group in photosystem I, J. Phys. Chem. B 116 (2012) 14008–14016.
[33] W. Lubitz, EPR studies of the primary electron donor P700 in photosystem I, in: J.H. Golbeck (Ed.), Photosystem I: The Light-Driven Plastocyanin:Ferredoxin Oxidoreductase, Springer, Dordrecht, The Netherlands, 2006, pp. 245–269.
[34] S. Santabarbara, I. Kuprov, W.V. Fairclough, S. Purton, P.J. Hore, P. Heathcote, M.C.W. Evans, Bidirectional electron transfer in photosystem I: determination of two distances between P(700)(+) and A(1)(−) in spin-correlated radical pairs, Biochemistry 44 (2005) 2119–2128.
[35] S.G. Zech, W. Hofbauer, A. Kamlowski, P. Fromme, D. Stehlik, W. Lubitz, R. Bittl, A structural model for the charge separated state $P_{700}^{\cdot+}A_1^{\cdot-}$ in photosystem I from the orientation of the magnetic interaction tensors, J. Phys. Chem. B 104 (2000) 9728–9739.
[36] R. Bittl, S.G. Zech, P. Fromme, H.T. Witt, W. Lubitz, Pulsed EPR structure analysis of photosystem I single crystals: localization of the phylloquinone acceptor, Biochemistry 36 (1997) 12001–12004.
[37] J. Biggins, P. Mathis, Functional-role of vitamin-K1 in photosystem-I of the *Cyanobacterium synechocystis*-6803, Biochemistry 27 (1988) 1494–1500.
[38] S.I. Ozawa, M. Kosugi, Y. Kashino, T. Sugimura, Y. Takahashi, 5′-Monohydroxyphylloquinone is the dominant naphthoquinone of PSI in the green alga *Chlamydomonas reinhardtii*, Plant Cell Physiol. 53 (2012) 237–243.
[39] R. Koradi, M. Billeter, K. Wüthrich, MOLMOL: a program for display and analysis of macromolecular structure, J. Mol. Graph. 14 (1996) 51–55.